

Lawrence Berkeley National Laboratory

Recent Work

Title

THE ANGULAR DISTRIBUTION AND YIELD OF THE PROCESS $p + d \rightarrow t + n$

Permalink

<https://escholarship.org/uc/item/4w08t1xx>

Author

Prank, Wilson J.

Publication Date

1953-05-18

UCRL 2292
UNCLASSIFIED

UNIVERSITY OF
CALIFORNIA

*Radiation
Laboratory*

TWO-WEEK LOAN COPY

*This is a Library Circulating Copy
which may be borrowed for two weeks.
For a personal retention copy, call
Tech. Info. Division, Ext. 5545*

BERKELEY, CALIFORNIA

DISCLAIMER

This document was prepared as an account of work sponsored by the United States Government. While this document is believed to contain correct information, neither the United States Government nor any agency thereof, nor the Regents of the University of California, nor any of their employees, makes any warranty, express or implied, or assumes any legal responsibility for the accuracy, completeness, or usefulness of any information, apparatus, product, or process disclosed, or represents that its use would not infringe privately owned rights. Reference herein to any specific commercial product, process, or service by its trade name, trademark, manufacturer, or otherwise, does not necessarily constitute or imply its endorsement, recommendation, or favoring by the United States Government or any agency thereof, or the Regents of the University of California. The views and opinions of authors expressed herein do not necessarily state or reflect those of the United States Government or any agency thereof or the Regents of the University of California.

UNIVERSITY OF CALIFORNIA

Radiation Laboratory

Contract No. W-7405-eng-48

THE ANGULAR DISTRIBUTION AND YIELD OF THE PROCESS



Wilson J. Frank

(Thesis)

May 18, 1953

Berkeley, California

TABLE OF CONTENTS

	Page
ABSTRACT	3
I. INTRODUCTION	4
II. KINEMATICS	4
III. DETAILS OF THE EXPERIMENT	
A. Apparatus	6
B. Method	7
IV. RESULTS OF THE EXPERIMENT	
A. Identification Data	9
B. Angular Distribution Data	11
C. Conclusions	14
V. ACKNOWLEDGMENTS	15
VI. APPENDICES	
A. Charge Independence of Nuclear Forces	16
B. Relativistic Calculation of the Kinematics	18
C. Corrections to the Data	21
1. Pion Decay in Flight	21
2. Pion Absorption	22
3. Small Angle Scattering	23
VII. REFERENCES	27
VIII. ILLUSTRATIONS	28

THE ANGULAR DISTRIBUTION AND YIELD OF THE PROCESS



Wilson J. Frank

Radiation Laboratory, Department of Physics
University of California, Berkeley, California

May 18, 1953

ABSTRACT

The angular distribution of the process $p + d \rightarrow t + \pi^+$ has been determined, using the 340 Mev proton beam from the Berkeley 184-inch synchrocyclotron. The process was identified at one angle by a comparison of measured and predicted angles of correlation, ranges of the particles, and time of flight of the triton. The same method was used at the other angles, with the apparatus set for the predicted correlated angles, minimum ranges, and triton time of flight; however, no further tests were made because of the low counting rates in the experiment. The results, corrected for pion absorption and decay in flight, and pion and triton multiple scattering, are as follows:

<u>Pion Center of Mass Angle</u>	<u>$\frac{d\sigma}{d\Omega}_0$ (microbarns/steradian)</u>
30°	3.95 ± 0.97
50°	2.55 ± 0.18
70°	0.77 ± 0.11
90°	0.44 ± 0.05
130°	0.46 ± 0.07
150°	0.41 ± 0.12

The errors given are statistical standard deviations. From this angular distribution, the total yield of the process is estimated to be 15 microbarns.

THE ANGULAR DISTRIBUTION AND YIELD OF THE PROCESS



Wilson J. Frank

Radiation Laboratory, Department of Physics,
University of California, Berkeley, California

May 18, 1953

I. INTRODUCTION

The process $p + d \rightarrow d + \pi^+$ is of interest for several reasons. One reason is that its relation to the analogous process $p + p \rightarrow d + \pi^+$ makes it somewhat amenable to theoretical treatment, and a prediction of its angular distribution and yield can be made.^{1, 2} This prediction involves some assumptions about the deuteron and triton wave functions and an estimate of the angular distribution and yield of the process $p + p \rightarrow d + \pi^+$ for pions with a center-of-mass energy of 78 Mev. Once the experimental data on the $p + d \rightarrow t + \pi^+$ process are available, the theoretical treatment can be reversed or modified to give some information on the estimates and assumptions used.

Another reason why the process $p + d \rightarrow t + \pi^+$ is of interest is that a comparison of it and its partner process $p + d \rightarrow \text{He}^3 + \pi^0$ would provide a stringent test^{1, 3} of the charge independence hypothesis. If nuclear forces are charge independent in this energy region where pions are produced, (see Appendix A), the angular distributions of these two processes should be identical, and their yields should have a ratio of 2:1.

II. KINEMATICS

The incident particles in the process $p + d \rightarrow t + \pi^+$ are the 340 Mev protons from the Berkeley 184-inch synchrocyclotron. For such a monoenergetic two-body process, the conservation equations for energy and momentum can be solved to give the correlated angles and energies of the resultant particles. An outline of a relativistic calculation is given in Appendix B; the results of this calculation are

summarized in Fig. 1. One important feature of this angular correlation curve is that the tritons are confined within a twelve-degree cone about the beam axis. In the analogous reaction $p + p \rightarrow d + \pi^+$, the deuterons are confined to a six-degree cone. The triton cone is larger because the extra target nucleon reduces the center of mass motion, which increases the effect of the triton momentum component perpendicular to the beam axis. A comparison of the two processes $p + d \rightarrow t + \pi^+$ and $p + p \rightarrow d + \pi^+$ is given in the following table:

TABLE I

	<u>$p + d \rightarrow t + \pi^+$</u>	<u>$p + p \rightarrow d + \pi^+$</u>
Threshold laboratory proton energy	210 Mev	290 Mev
Energy available with 340 Mev incident protons	219 Mev	163 Mev

The concentration of tritons within a small angular region in the forward direction makes possible a triton time-of-flight measurement without a sacrifice in counting rate. For example, consider the correlated angles of 8.0° for the triton and 110° for the pion. In this region of Fig. 1, a nine-degree center-of-mass angular interval for tritons is compressed into a one-degree laboratory angular interval; in the same transformation, the pion angular interval is changed only slightly. If the distance of the triton counters from the target is nine times that of the pion counters, then triton and pion counters of the same horizontal dimensions will subtend the same center-of-mass angular interval. Even though the triton counters are considerably farther from the target than the pion counters, both sets of counters will be about the same perpendicular distance from the beam axis; therefore, triton and pion counters of roughly the same vertical dimensions will intercept the same azimuthal angular interval. This fact is illustrated in Fig. 2. In summary, the solid angle determined by the pion counters at a distance of fourteen inches from the target is not reduced by placing similar-sized triton counters eleven feet from the target. This large triton counter distance allows the triton time of flight to be measured.

III. DETAILS OF THE EXPERIMENT

A. Apparatus

The experimental arrangement at a typical angle is illustrated in Fig. 2. The incident 340 Mev protons were collimated to a two-inch diameter beam. The beam was monitored by an ionization chamber; ion current was integrated on a calibrated condenser and recorded in units of volts by a recording millivoltmeter. The targets of deuterated paraffin (CD_2) and carbon (C) were three inches in diameter and contained the same number of carbon atoms. The particle detector at the triton angle consisted of two trans-stilbene phosphors; each phosphor was two inches by four inches and was viewed by two 1P21 photomultiplier tubes. The phosphor thicknesses were selected so that the expected tritons, after suitable absorber, would lose 20 to 30 Mev in each. The two signals from a given phosphor are shaped by clipping to a width of three millimicroseconds and added together. Trans-stilbene phosphors were used because their rise time is of the order of millimicroseconds; thus, not as much of the pulse energy is lost by shaping as would be with some other commonly used phosphors. Fig. 3 shows this shaper-adder-limiter circuit together with the last dynode stage of the photo multiplier. The 259 ohm coaxial cable was used to increase the signal transmitted from the photo multiplier and help eliminate the need for amplifiers between the photo multiplier and the coincidence circuit.

The particle detector at the pion angle consisted of two trans-stilbene phosphors; each phosphor was two inches square and was viewed by one 1P21 photomultiplier tube. The phosphor thicknesses were selected so that the expected pions, after suitable absorber, would lose 10 to 15 Mev in each. Each pion signal is clipped to a width of three millimicroseconds and delayed by the length of coaxial line calculated to match the expected triton signal time of arrival at the coincidence circuit. The two triton signals and the two delayed pion signals are fed into a germanium diode quadruple coincidence circuit having a resolution time of about three millimicroseconds with these pulses. Fig. 4 is a schematic diagram of the coincidence circuit. The IN38 germanium diode inputs were used instead of tubes to increase the circuit sensi-

tivity and eliminate input signal amplifiers. The three parallel IN56 diodes and the associated capacitor are due to Garwin⁴. They increase the discrimination ratio by clamping the output voltage in all cases in which less than four of the input diodes are cut off.

The IN54A diode in the grid of the output tube was introduced to increase further the discrimination of the circuit. A typical ratio of quadruple to triple coincidence output pulse heights is around twenty to thirty. The output signal of the coincidence circuit is amplified, and recorded on two scaling units with different bias settings. This procedure provides a measure of the bias plateau that cannot be obtained because of the low counting rates. The efficiency of the counting equipment has been measured to be almost one hundred percent. A more detailed account of the electronic equipment is being published by Richard Madey, who was the leader in its development.

B. Method

Because of the low counting rates in this experiment, the process $p + d \rightarrow t + \pi^+$ was identified by a number of tests at only one angle. However, at each angle, three conditions were placed on the coincidences observed: (1) the counters were set at a given pair of correlated angles; (2) a time of flight requirement was placed on the triton by delaying the pion signals relative to the triton signals according to the calculated relative velocities; (3) the absorbers added to each counter telescope were selected to stop any particles with ranges below the minimum calculated ranges.

The 340 Mev scattered deflected external proton beam of the Berkeley synchrotron has an envelope of roughly twenty-five microseconds duration, which is repeated about sixty times a second. Within this envelope, a fine structure exists with the sixteen megacycle frequency of a phase stable bunch of protons circulating near the machine maximum radius. Thus, the fine structure interval between proton pulses is about sixty millimicroseconds; the width at half maximum of a single pulse of protons is about four millimicroseconds⁵. The bunched protons in the beam produce bunched background, such as elastically scattered protons and deuterons, which have cross-sections

several orders of magnitude above the cross section of the process $p + d \rightarrow t + \pi^+$. However, the time-of-flight method used for measuring the triton velocity can also be used to separate the background processes by means of their different velocities and reduce accidental counts caused by them.

The time-of-flight method will discriminate only against background particles with velocities different enough from the expected triton velocity to separate the two particle groups at the triton counter by a time comparable to the resolution time of the coincidence circuit. For background such as protons and deuterons with velocities similar to the expected triton velocity, an absorption, or range, method can be used, since these protons and deuterons have one-third and two-thirds, respectively, the range of tritons of the same velocity. By adding enough absorber before a counter telescope to stop the expected particle at the back of the last phosphor, most of the similar velocity background can be eliminated.

The calculations for a typical angle will be used to illustrate the method more specifically. For the case of a pion center-of-mass angle of 130° , the laboratory correlated angles are 8.0° for the triton and 110° for the pion. The triton energies are double-valued, but the pion angle requirement eliminates one possibility. This geometry is shown in Fig. 2. Suppose a time origin is taken when a proton pulse passes through the target and assume that a triton-pion or a miscellaneous pair of background particles are created somewhere within the proton pulse envelope. The triton-pion are created simultaneously, but the background pair occur separately, spaced at most by the envelope width. (This condition is somewhat idealized, but surely most of the background trouble arises from the many protons in the peak of the pulse rather than from the few protons in the tail.) The pion velocity at 110° is $.69c$ (c is the velocity of light), and the pion arrives at its counter in 2 millimicroseconds. The pion counter background is slower, except for electrons and gamma rays, but is not debunched much over the short distance from target to counter. The time sequence of events being described is illustrated in Fig. 5. The triton velocity at 8.0° is $.31c$, while the

velocity of elastically scattered protons is about .67c. Over the eleven feet from target to counters, the probability envelopes of these two particles are separated by about twenty millimicroseconds. By delaying the pion counter signals with an amount of delay line calculated from the pion-triton expected time of flight, the real pion-triton counts are placed in coincidence. The pion counter background is well separated from the fast triton counter background, and possible accidental coincidences are discriminated against by the 3 millimicrosecond resolving time of the coincidence circuit.

Absorbers calculated to stop the expected particle at the back of the last phosphor were added to each counter telescope in order to increase the energy loss in the phosphor, enhance its efficiency, and reduce counts due to low energy background. The aluminum absorber calculated for tritons at 8.0° will stop 85 Mev protons. Fig. 5 shows that protons of this energy and greater are in the fast background category and discriminated against by the coincidence circuit resolving time.

The method in summary, then, is this: two particles are detected in coincidence at angles correlated for the process $p + d \rightarrow t + \pi^+$; greater velocity background is eliminated by a time-of-flight requirement; similar velocity background is eliminated by a range requirement. The success of the method is seen in the fact that a CD_2 to C ratio of 5:1 was obtained at most angles without using unreasonably low beam intensities.

IV. RESULTS OF THE EXPERIMENT

A. Identification Data

When the method described above was first developed, a number of identification tests were made at one angle in order to be certain that the process $p + d \rightarrow t + \pi^+$ was really being observed. A summary of these tests will be given in this section.

First, a difference in the coincidence counting rates from CD_2 and C targets was obtained at the correlated laboratory angles of 8.0° for the triton and 110° for the pion, and with the calculated ab-

sorbers and delay lines. The result of varying the proton beam intensity is given in Table II.

Table II

Relative Beam Intensity	CD ₂ -C Difference Rate	CD ₂ to C Ratio
6	1.00 ± 0.20	3:1
1	1.25 ± 0.30	6:1

The counting rate units are counts per unit of integrated beam. The target out counting rate was a factor of five below the carbon rate at the higher intensity. The fact that the difference counting rate is constant over a large variation in intensity indicates that a real process from protons on deuterons is being observed. The identification tests of this real process are made by changing the angles, absorbers, and delay lines from the calculated values and observing the reduction in the difference counting rate.

The angular correlation of the process was tested by moving each counter telescope separately from its calculated angle. The results, plotted in Fig. 6, show that the difference was properly reduced in each case. Both sets of counters subtended the same center-of-mass angles, but the pion counters were moved two counter widths to each side while the triton counters were moved three counter widths. This fact plus the two-inch beam width and the large triton scattering make plausible the incomplete counting rate disappearance when the pion counters were moved. The co-planarity of the process was tested by raising the triton counters one counter height out of the plane formed by the beam axis and the pion counters; the difference dropped to 0.00 ± 0.30 from the normal 1.00 ± 0.20 counts per integrated beam unit.

The time-of-flight correlation of the process was tested by changing the arrival time of the pion signal relative to the triton signal. The results of varying the length of pion delay line are given in Fig. 7. The difference counting rate is a maximum when the length of delay line in the pion counters is chosen to match the expected

triton velocity; the difference rate disappears for particle velocities larger or smaller by twelve percent. The effectiveness of the time-of-flight and range method in reducing background counts may be appreciated by noting how rapidly the carbon counting rate rises as delay is removed between the pion counters and the coincidence circuit. The reason for the rise in this accidental coincidence rate can be understood from Fig. 5; the shorter delay allows the pion counter background to synchronize with the faster triton counter background.

The ranges of the particles causing the coincidences were measured. The range spectrum of the particles passing through the triton counters and participating in a coincidence is shown in Fig. 8; the calculated triton ranges are indicated for comparison. The spread in the expected ranges is caused by production at different target depths. The measured range agrees with the calculated triton energy to within ten percent. The effectiveness of the range method in reducing accidental coincidences due to similar velocity background is illustrated by the fact that the CD_2 to C ratio of three to one with the absorber drops to four to three without the absorber. The range of the particles at the pion counters participating in coincidences was measured by adding more absorber to the pion counters; the measured range agrees with the predicted pion energy to within ten percent.

These identification tests show a real process from the deuteron, or one of its components; this process is a monoenergetic two-body reaction that is consistent with the process $p + d \rightarrow t + \pi^+$. Because of the low counting rates in this experiment, such a series of tests cannot be made for each angle without excessive use of cyclotron time. The general method of imposing the conditions of correlated angles, expected triton time-of-flight, and minimum ranges for both particles was extended to the other angles at which cross sections were obtained, but no further tests were made.

B. Angular Distribution Data

Data for an angular distribution were taken at six laboratory angles chosen to correspond to equally spaced angles in the center-of-mass system. These uncorrected data are summarized in Table III.

Table III

<u>Pion CoM Angle</u>	<u>Difference of CD₂ and C Rates</u>	<u>Ratio of CD₂ to C Rates</u>
30°	1.79 ± 0.44	6
50	5.95 ± 0.40	10
70	2.85 ± 0.40	9
90	1.56 ± 0.16	15
130	0.98 ± 0.13	4
150	0.62 ± 0.17	2

Three corrections were applied to the original difference counting rate. The first is due to the decay of the pions in flight; it is small because of the short flight path and is only a few percent at most. The second is caused by absorption of the pions in passing through the copper absorbers in the pion counter telescope. At most, thirty percent of the pions are lost because of the minimum range requirement. The third and largest correction is due to small angle scattering. It is the price paid for the time of flight aid in identifying the process and suppressing the background. At worst, however, less than fifty percent of possible coincidences are lost. The correction factors are summarized in Table IV; fuller details on these corrections are given in Appendix C.

Table IV

<u>Pion CoM Angle</u>	<u>Decay</u>	<u>Absorption</u>	<u>Scattering</u>	<u>Total</u>
30°	1.03	1.43	1.32	1.94
50	1.03	1.40	1.54	2.21
70	1.03	1.26	1.73	2.24
90	1.03	1.19	1.80	2.21
130	1.05	1.05	1.65	1.82
150	1.06	1.02	1.54	1.66

The center of mass differential cross-section is obtained from the relation

$$\frac{d\sigma}{d\Omega_0} = \frac{RC}{N_b N_t \Delta\Omega_0}$$

The numerator is the product of the original difference rate, R, and the total correction factor, C. N_b is the proton beam flux in protons per integrated beam unit; it is calculated from the ion chamber calibration factor and the integrating condenser value. N_t is the target particle density in deuterons per square centimeter; it depends on the weight, area, and composition of the target and the angle the target makes with the beam direction. $\Delta\Omega_0$ is the center of mass solid angle subtended by the smallest counter; it is calculated from the laboratory solid angle by means of the transformations in Appendix B. The final results are given in Table V and plotted in Fig. 9.

Table V

<u>Pion CoM Angle</u>	<u>$\frac{d\sigma}{d\Omega_0}$ (microbarns/steradian)</u>
30°	3.95 ± 0.97
50	2.55 ± 0.18
70	0.77 ± 0.11
90	0.44 ± 0.05
130	0.46 ± 0.07
150	0.41 ± 0.12

The errors shown are the statistical standard deviations related to the number of counts obtained in the original data. The errors in N_b , N_t , and $\Delta\Omega_0$ have been neglected as far as this relative angular distribution data is concerned, since they are the same for each angle and affect only the total absolute cross-section. The error in N_b is estimated to be several percent; in N_t , about one or two percent;

and in $\Delta\Omega_0$, somewhere between five and ten percent; together N_b , N_t , and $\Delta\Omega_0$ will add ten to fifteen percent uncertainty to the total cross-section. By drawing a reasonably smooth curve through the data of Fig. 9, the integrated total cross-section is estimated to be fifteen microbarns. Since the counter and coincidence equipment is nearly one hundred percent efficient, this total cross-section can be taken as the absolute yield with a probable error in the region of twenty-five percent.

C. Conclusions

The process $p + d \rightarrow t + \pi^+$ has been considered from a theoretical viewpoint by Ruderman¹ and Bludman². The angular distribution is derived in terms of the cross-section of the process $p + p \rightarrow d + \pi^+$, by making some simplifying assumptions. From the evidence of the high π^+/π^- ratio for protons on deuterium⁶ and carbon⁷ and the low π^+/π^- ratio for neutrons on carbon⁸, it is assumed that in the process $p + d \rightarrow t + \pi^+$ the incident proton interacts with the proton rather than the neutron in the deuteron to produce the pion; the two protons form a deuteron and a pion. If the neutron, which is assumed to have been a spectator thus far, has the proper momentum, it can form a triton with the new deuteron. The triton wave function is approximated in terms of the deuteron wave function by assuming the separation of the nucleons producing the pion small compared to their separation from the spectator neutron. The result $d\sigma/d\Omega_0(p + d \rightarrow t + \pi^+)$ then depends on the deuteron and triton wave functions, as well as upon $d\sigma/d\Omega_0(p + p \rightarrow d + \pi^+)$. This value of the angular distribution and yield for the process $p + p \rightarrow d + \pi^+$ is taken for pions with a center-of-mass energy of 78 Mev, which is the center-of-mass pion energy in the process $p + d \rightarrow t + \pi^+$. The $d + \pi^+$ cross-section was extrapolated from Berkeley⁹ and Columbia¹⁰ data to be $210(1/3 + \cos^2\theta)$ microbarns/steradian for the differential cross-section and 1.8 millibarns for the total cross-section. The $t + \pi^+$ angular distribution is relative, however, and depends only on the $d + \pi^+$ angular distribution, and not its total cross-section. Using the above $d + \pi^+$ cross-section and the ordinary Hulthen deuteron wave function, the theoretical

result labelled "no core" in Fig. 10 is obtained. This curve does not agree with the marked flat distribution from 90° to 180° of the experiment. The curve could be flattened somewhat by choosing a more isotropic angular distribution for the $p + p \rightarrow d + \pi^+$ process; however, the present data do not seem to indicate such a trend. The curve can also be flattened by reducing the high momentum components of the deuteron wave function, which can be done by introducing a core model of nuclear forces. The nucleon model of a short-range repulsive force core surrounded by the usual longer-range attractive well was originally introduced by Jastrow¹¹ to reconcile the hypothesis of charge independence with the qualitative features of high energy n-p and p-p scattering. The results of choosing nucleon cores at radii of 0.38 and 0.50 pion Compton wave lengths are shown in Fig. 10. The agreement of the experimental data with a core of 0.50 is striking; however, because of the approximations made, the conclusion can be only that a core model of nuclear forces is consistent with the experimental results.

V. ACKNOWLEDGMENTS

I would like to thank the many persons who have aided in completing this experiment. Burton J. Moyer has been most helpful with his counsel and encouragement during my graduate career. Kenneth Bandtel and Richard Madey have been partners in developing the experiment and obtaining the data. Paul Nikonenko has put much work into the electronics equipment. Sidney Bludman and Malvin Ruderman have helped in providing a theoretical interpretation. The Radiation Laboratory and James Vale and the cyclotron crew have provided the means for doing the experiment.

VI. APPENDICES

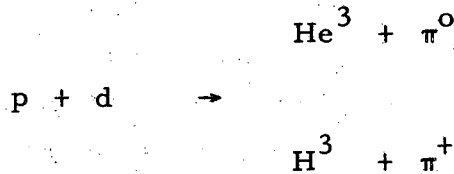
A. Charge Independence of Nuclear Forces

Shortly after the discovery of the neutron, Heisenberg introduced the idea that the neutron and proton might be different charge states of a particle to be called the nucleon. A new quantum number, designated by τ and called the isotopic spin, was defined in analogy to ordinary spin. Just as the ordinary spin of a particle can be determined by its multiple structure in a magnetic field, a particle's isotopic spin is revealed by the splitting caused by a coulomb field. The projection of τ on the third axis in isotopic spin space gives the charge state of the particles. Since the nucleon has a doublet structure, it is assigned $\tau = 1/2$, with $\tau = +1/2$ for a proton and $\tau = -1/2$ for a neutron. The pion has a triplet structure since positive, negative, and neutral pions have been discovered and studied; therefore, the pion is assigned $\tau = 1$, with $\tau_3 = +1, 0, -1$ for positive, neutral, and negative pions respectively. The Pauli principle for neutrons and protons can be extended to nucleons by requiring that the total wave function (including the space, spin, and isotopic spin components) be antisymmetric. Thus, two protons, or two neutrons, are in a symmetric isotopic spin state with $T = 1$; if they are in an S space state, which is also symmetric, their spin state must be anti-symmetric with $S = 0$. A neutron and a proton could have either $T = 1$ or $T = 0$; for an S space state, the isotopic spin $T = 1$ state must go with the ordinary spin $S = 0$ state, and the $T = 0$ state with the $S = 1$ state. Thus, the deuteron ground state has $T = 0$.

Charge symmetry of nuclear forces assumes that the p-p and n-n forces are equal insofar as the interaction is transmitted by the pion field. The charge independence hypothesis extends this equality to include n-p forces; that is, nucleon-nucleon interactions are equal for the same space, spin, and isotopic spin state. If the Hamiltonian is unchanged by a rotation in coordinate space, it commutes with the angular momentum, and the angular momentum is a constant of the motion. Similarly, if the Hamiltonian is unchanged by a rotation in isotopic spin space, it will commute with the total isotopic spin, and the total isotopic spin will be a constant of the motion. If the Hamil-

tonian is unchanged by rotation in isotopic spin space, it cannot contain any isotopic spin operators (except for scalars like T^2) to distinguish between different kinds of nucleons or pions. Thus, the consequences of charge independence can be investigated by assuming the total isotopic spin, T , is a constant of the motion. T_3 is also a constant of the motion because of the conservation of charge.

If a proton with $T = 1/2$, $T_3 = 1/2$ is incident on a deuteron with $T = 0$, $T_3 = 0$, the resultant isotopic spin state will be $T = 1/2$, $T_3 = 1/2$. If charge independence of nuclear forces holds in this energy region (340 Mev incident protons), the final state must also have $T = 1/2$, $T_3 = 1/2$. A comparison of the cross-sections of two possible final states can be used to test the charge independence hypothesis. The two processes are:



Some of the first evidence for charge symmetry was obtained in a study of the mirror nuclei H^3 and He^3 ; such properties as their spins, magnetic moments, binding energies, and so forth, make plausible the assumption that the spin and space parts of their two ground state wave functions are the same. It will be assumed further that these two nuclei represent the two charge states of a tri-nucleon group of isotopic spin $T = 1/2$. Since pions are also different charge states of the same particle, the two states He^3, π^0 and H^3, π^+ are identical except for the arrangement of the charges. One state could be transformed into the other by a suitable rotation in isotopic spin space. If then the assumption of charge independence is mostly correct, the two processes should have the same angular distributions. The ratio of the total cross-sections or the differential cross-sections at any angle, will depend on the mixture ratio of the states in the $T = 1/2, T_3 = 1/2$ eigenfunction. The procedure is exactly analogous to finding the eigenfunctions for a single electron in a P state, and in particular, the eigenfunction for the ${}^2P_{1/2}$ state with $m = 1/2$. Let I_T^3 represent the isotopic spin eigenfunction; N_T^3 , the He^3, H^3 functions; and π_T^3 , the pion functions.

The final state, then, can be written

$$I_{1/2} = aN_{-1/2} \pi_1 + bN_{1/2} \pi_0$$

By applying the operators T^2 and T_3 , which are analogous to J^2 and J_z , the coefficients are found to be $a = \sqrt{2/3}$ and $b = \sqrt{1/3}$. This result means that the ratio of the H^3 to He^3 cross-sections is two to one.

B. A Relativistic Calculation of the Kinematics

The following notation is used: the rest mass of a particle is $M = m_0 c^2$, its velocity is $\beta = v/c$, and γ is defined as $(1 - \beta^2)^{-1/2}$; the particle's kinetic energy is T , and its total energy is $E = T + M = \gamma M$; its momentum is $P = cp = c\gamma m_0 v = \gamma \beta M$; E , T , P , and M are given in units of Mev. Some relativistic relations between these quantities are: $E^2 = P^2 + M^2$; $P^2 = T(T + 2M)$; $P = \beta E$; and $\beta^2 + \gamma^{-2} = 1$. This last equation is satisfied if we put $\beta = \sin \theta$ and $\gamma = \sec \theta$, or $\beta = \tanh \phi$ and $\gamma = \cosh \phi$; a table of either of these pairs of functions can be used to evaluate β or γ if one of them is known. Furthermore, since $P = \gamma \beta M$ and $\gamma \beta = \tan \theta$, or $\sinh \phi$, P can be calculated easily if it is desired.

If the quantities E , P , M of a particle are known in one system of reference and E_0 , P_0 , M_0 are desired in a second system of reference moving parallel to the particle and having a velocity β_0 with respect to the first system, these transformation equations are used: $E = \gamma_0 (E_0 + \beta_0 P_0)$; $P = \gamma_0 (P_0 + \beta_0 E_0)$; $E_0 = \gamma_0 (E - \beta_0 P)$; $P_0 = \gamma_0 (P - \beta_0 E)$. If the direction of the particle is not parallel to the relative velocity β_0 , but makes an angle θ with it in the first system and an angle θ_0 in the second system, the transformation equations become: $E = \gamma_0 (E_0 + \beta_0 P_0 \cos \theta_0)$; $P \cos \theta = \gamma_0 (P_0 \cos \theta_0 + \beta_0 E_0)$; $E_0 = \gamma_0 (E - \beta_0 P \cos \theta)$; $P_0 \cos \theta_0 = \gamma_0 (P \cos \theta - \beta_0 E)$; and $P \sin \theta = P_0 \sin \theta_0$. Usually the first frame of reference is the laboratory system in which a particle of known energy is incident upon a target particle at rest. The second frame of reference is normally taken to be the center-of-mass system, which might better be called the center-of-momentum system, since it

is that frame in which the vector sum of the momenta is zero. For notation, let the subscript 1 designate the incident particle and 2 the target particle; the total energy in the laboratory system is then $E = E_1 + E_2 = E_1 + M_2$; the total momentum is $P = P_1$. If E_0 and P_0 are the total energy and momentum in the center-of-mass system, then $P_0 = 0$ by definition. The transformation equations are then: $E = \gamma_0 E_0$ and $P = \beta_0 E_0$. Thus, E_0 can be easily evaluated and used to get the energy available for any possible process resulting from the interaction of the two initial particles.

In many processes of interest, such as the present one, $p + d \rightarrow t + \pi^+$, there are only two particles in the final state. For such a case, the conservation equations for energy and momentum lead to correlated angles and energies for the two resultant particles. Let these particles be designated by the subscripts 3 and 4; they will make angles θ_3, θ_4 with the beam axis. In the center-of-mass system, the additional subscript 0 will be added to distinguish this frame of reference. The sequence of formulae used in calculations for a two-body process like $p + d \rightarrow t + \pi^+$ is summarized below:

1. The available energy in the center-of-momentum system.

The total laboratory energy is $E = E_1 + E_2 = T_1 + M_1 + M_2$

The total laboratory momentum is $P = P_1 + P_2 = P_1 = [T_1(T_1 + 2M_1)]^{1/2}$

The transformation velocity is $\beta_0 = P/E$; γ_0 and $\gamma_0\beta_0$ are gotten from hyperbolic function tables.

The total c-o-m-energy is $E_0 = E/\gamma_0$, while the available energy is $Q = E_0 - M_3 - M_4$.

2. The constants, E, P, β , γ for a center-of-mass particle.

The conservation equations in the center-of-mass system are

$$E_{04} = E_0 - E_{03} \quad \text{or} \quad E_{04}^2 = E_0^2 - 2E_0 E_{03} + E_{03}^2$$

$$P_{04} = P_{03} \quad \text{or} \quad E_{04}^2 - M_4^2 = E_{03}^2 - M_3^2$$

Subtracting the two equations and solving for E_{03} gives

$$E_{03} = \frac{E_0^2 + M_3^2 - M_4^2}{2E_0}$$

The other constants can be gotten in several ways from E_{o3} by the relativistic relations and the hyperbolic function tables, so that γ_{o3} , β_{o3} , and P_{o3} are known. From $P_{o3} = P_{o4}$, the constants γ_{o4} , β_{o4} , P_{o4} , and E_{o4} can be calculated. Or they can be calculated by the above method as a cross check.

3. The laboratory correlated angles and energies of the resultant particles.

The result of dividing the perpendicular component transformation equation, $P_3 \sin \theta_3 = P_{o3} \sin \theta_{o3}$, into the parallel component equation, $P_3 \cos \theta_3 = \gamma_o (P_{o3} \cos \theta_{o3} + \beta_o E_{o3})$

$$\text{is } \cot \theta_3 = \gamma_o \left[\cot \theta_{o3} + \frac{\beta_o}{\beta_{o3}} \csc \theta_{o3} \right]$$

The constants γ_o , β_o , and β_{o3} are known so that values of θ_3 can be found for any series of center-of-mass angles θ_{o3} . Once θ_3 is known, P_3 can be found from

$$P_3 = P_{o3} \frac{\sin \theta_{o3}}{\sin \theta_3}$$

and used to calculate E_3 , β_3 , γ_3 , T_3 , or as many of these quantities as may be needed. The laboratory quantities for particle 4 can be evaluated in the same way.

4. The solid angle transformation from the laboratory system to the center-of-mass system.

$$\text{In the equation } \cot \theta_3 = \gamma_o \left[\cot \theta_{o3} + \frac{\beta_o}{\beta_{o3}} \csc \theta_{o3} \right],$$

the only variables are θ_3 and θ_{o3} while the constants γ_o , β_o , β_{o3} have been calculated. Differentiating this equation gives:

$$-\csc^2 \theta_3 \frac{d\theta_3}{d\theta_{o3}} = \gamma_o \left[-\csc^2 \theta_{o3} - \frac{\beta_o \csc \theta_{o3} \cot \theta_{o3}}{\beta_{o3}} \right]$$

$$\text{or } \frac{d\theta_3}{d\theta_{o3}} = \gamma_o \frac{\sin^2 \theta_3}{\sin^2 \theta_{o3}} \left[1 + \frac{\beta_o \cos \theta_{o3}}{\beta_{o3}} \right]$$

The center-of-mass solid angle is given by

$$\Delta\Omega_{o3} = \sin\theta_{o3} \Delta\theta_{o3} \Delta\phi = \frac{\sin\theta_{o3}}{\sin\theta_3} \sin\theta_3 = \Delta\theta_3 \frac{d\theta_{o3}}{d\theta_3} \Delta\phi$$

or

$$\Delta\Omega_{o3} = \frac{\sin\theta_{o3}}{\sin\theta_3} \frac{d\theta_{o3}}{d\theta_3} \Delta\Omega_3$$

$$\Delta\Omega_{o3} = \frac{\sin^3\theta_{o3} \Delta\Omega_3}{\gamma_o \sin^3\theta_3 \left(1 + \frac{\beta_o \cos\theta_{o3}}{\beta_{o3}} \right)}$$

C. Corrections to the Data

1. Pion Decay in Flight. For experiments in which the π^+ meson is identified by its decay into a μ^+ meson, the correction for loss of pions by decay in flight is relatively simple. If the initial number of pions leaving the target is n_o , then the number arriving at the detector is $n = n_o e^{-t/\tau'}$. The mean life, τ , of charged pions in their rest frame is 26 millimicroseconds.¹² In the laboratory, the mean lifetime, τ' , is longer due to the relativistic time dilation effect and is equal to $\gamma\tau$, where γ is calculated from the pion laboratory velocity, β . The time of flight, t , of the pion over the distance, d , from the target to the detector is given by $t = d/\beta$. Thus, if n pions are detected, the number produced in the target is $n_o = n e^{d/\gamma\beta\tau}$.

In the present experiment, $p + d \rightarrow t + \pi^+$, the pion is being detected only as a charged particle satisfying the correlated angle, minimum range, and time of flight requirements. The muon decay product is charged and can also produce a coincidence providing it meets these requirements. To find the proportion of these muons that are not detected, consider the decay in the pion's rest frame. The muon has an energy of four Mev and a velocity β of about .25. A pion with a typical energy of 72 Mev and a laboratory velocity of $\beta = .75$ was

used to calculate the following table of muon angles, energies, and velocities.

<u>Center-of-mass decay angle</u>	<u>Laboratory decay angle</u>	<u>Laboratory kinetic energy</u>	<u>Laboratory velocity</u>
180°	0°	27 Mev	.60
120	14	44	.70
90	13	60	.77
60	10	75	.82
0	0	94	.85

A typical distance for the pion counter telescope is thirteen inches. Over this distance, the greatest difference between the times of flight of a pion and a muon decay product is less than a millimicrosecond; thus, all the decay muons can meet the time of flight requirement.

A pion with a $\beta = .75$ has a range of 24 grams/cm² in copper. Allowing for a twenty Mev loss in the final phosphor reduces this absorber to 21 g/cm². However, this amount will stop 60 Mev muons; thus, muons from the backward center-of-mass hemisphere fail to meet the minimum range requirement.

The cotangents of 10° to 13° are around five. The half width of the pion counter phosphors is an inch; only those decays five inches or less from the phosphor will be intercepted. It is estimated that about half of the muons from the forward center-of-mass hemisphere fail to meet the correlated angle requirement for this reason. It would be unprofitable to do an exact calculation for each pion angle, since the correction would be only six percent in the worst case if all the muons were lost. In this example, about three-quarters of the decay muons are not detected; for simplicity, it will be assumed that this figure holds at all the pion angles observed in the present experiment.

2. Pion Absorption. Because of the minimum range requirement on the pion, the pion passes through an appreciable amount of copper absorber before being detected. Some of the pions will interact with the copper nuclei and be absorbed or scattered at large angles. Usually this

interaction is assumed to be independent of the pion energy, so that the number of pions before absorption is $n_0 = n e^{\mu t}$; n is the number of pions counted, t is the thickness of the copper absorber in radiation lengths, and μ is the absorption coefficient in units of (radiation lengths)⁻¹. The absorption coefficient μ is given by

$$\sigma \frac{N_0}{A} (13.245)$$

in which N_0 is Avogadro's number, A is the molecular weight, 13.245 is a conversion factor from grams/(centimeter)² to radiation lengths of copper, and σ is the cross section for absorption. However, recent measurements by Stork¹³ show that σ is not a constant, but a function of the pion energy. Stork measured pion attenuation by absorption and scattering greater than 35° - a condition similar to placing absorber in front of an equal-sized counter. His results give a nuclear area cross-section above 85 Mev with a smaller cross section for decreasing energy. In this case, the exponent of e becomes an integral

$$\int_{t_1}^{t_2} \mu dt.$$

By plotting Stork's data in the form of μ versus t , this integral can be evaluated numerically to give the correction to the data.

3. Small Angle Scattering. In passing through matter, a charged particle will undergo a large number of small angle scatters due to Coulomb interaction with the charge on the nuclei. These numerous small deviations can be treated statistically to give the resultant distribution of angles or displacements; the distributions are usually gaussian and characterized by the mean square scattering angle or displacement. Later on, several formulae for these mean square angles and displacements will be given; the initial work was done by Williams¹⁴, and summarized and extended by Rossi and Greisen¹⁵ and Eyges¹⁶ for various conditions of application.

If only one of the resultant particles were being detected in the present experiment, $p + d \rightarrow t + \pi^+$, the small angle scattering

correction would be small since about as many particles would scatter into the detector as would be scattered away from it. By detecting both resultant particles in coincidence, the correction is increased because it is more likely that one or both of the particles will be scattered away from their counters than that both of the particles will be scattered into their respective counters. The usual solution to this problem involves making counters of one of the particles govern the subtended solid angle while enlarging counters of the other particle enough to collect all possible scattered coincidence-causing particles. This procedure is difficult in the present experiment because of the unusual angular correlation curve and the low counting rates. For example, suppose the pion and triton counters subtend equal correlated angular intervals. If then the triton counter is enlarged, background counts increase at a more or less constant rate while the extra coincidence counts occur at a diminishing rate; although the actual counting rate increases, the background difficulties increase more rapidly. If the pion counter is enlarged, troubles arise in the pion angle region near 70° (see Fig. 1); here the slope of the correlation curve goes through zero and unreasonably large pion counters would be needed. The difficulty of the greater background increase over the real count increase probably would not be as serious as in the triton case. For these reasons, the counters subtend on the average almost equal correlated angular intervals; the actual ratio depends on the angles, since the same counters are used at each chosen pair of angles.

In the formulae shown below, the following notation is used: P is the relativistic momentum in Mev; β is the velocity of the particle in units of the velocity of light; E_g is a combination of constants equal to 21.2 Mev. The thickness of the matter, t , is measured in radiation lengths which are constant for a given material and allow the formulae to be expressed more simply; t_0 is used for the range equivalent of the particle's initial energy. For greater utility, the mean square scattering angles or displacements are expressed in terms of their projections on a plane containing the particle's original direction.

There are three different situations in which small angle scattering calculations were made. The first involves scattering in the target. Here the energy loss is taken to be negligible and the effects of displacement in the target are small compared to those from possible angular deviation from the original direction. The mean square projected scattering angle is $\langle \theta^2 \rangle_{av} = E_s^2 t / 2P^2 \beta^2$. Target scattering is important for the tritons at all angles because of the large triton counter distance; it is less important for the pions, but it must be taken into account for pion angles around 90° where the pion travels through an appreciable amount of target material (refer to the experimental arrangement in Fig. 2). The second situation involves scattering in the air. Again energy loss is considered negligible; in this case, the displacement at the back edge of the absorber (the air) is more important than the angular distribution of the particles at that point. The mean square projected displacement is $\langle y^2 \rangle_{av} = E_s^2 t^3 / 6P^2 B^2$. Air scattering is almost of the same importance as target scattering for the triton; for the pion, it is negligible. The third situation involves scattering in the absorbers added to the counters to give the minimum range requirements. Energy loss is not negligible in this case, so that the calculation involves integration. The mean square projected displacement at the back edge of the absorber is

$$\langle y^2 \rangle_{av} = 2 \int_0^t \frac{(t-\eta)^2 d\eta}{W^2 (t_0 - \eta)}$$

where $W = 2P\beta/E_s$. Absorber scattering is negligible for the triton compared to the other two types of scattering; for the pion, it is comparable to target scattering at 90° .

The displacements are in terms of radiation lengths; in order to add the scattering effects, the displacements should be converted to effective angles by using a conversion factor from radiation lengths to centimeters and dividing by the counter-to-target distance. The scattering effects are compounded by adding the projected mean square angles for the three types of scattering. If the limits of the phosphor are given by θ_1 and θ_2 , then a function $h(\theta)$ can be calculated and

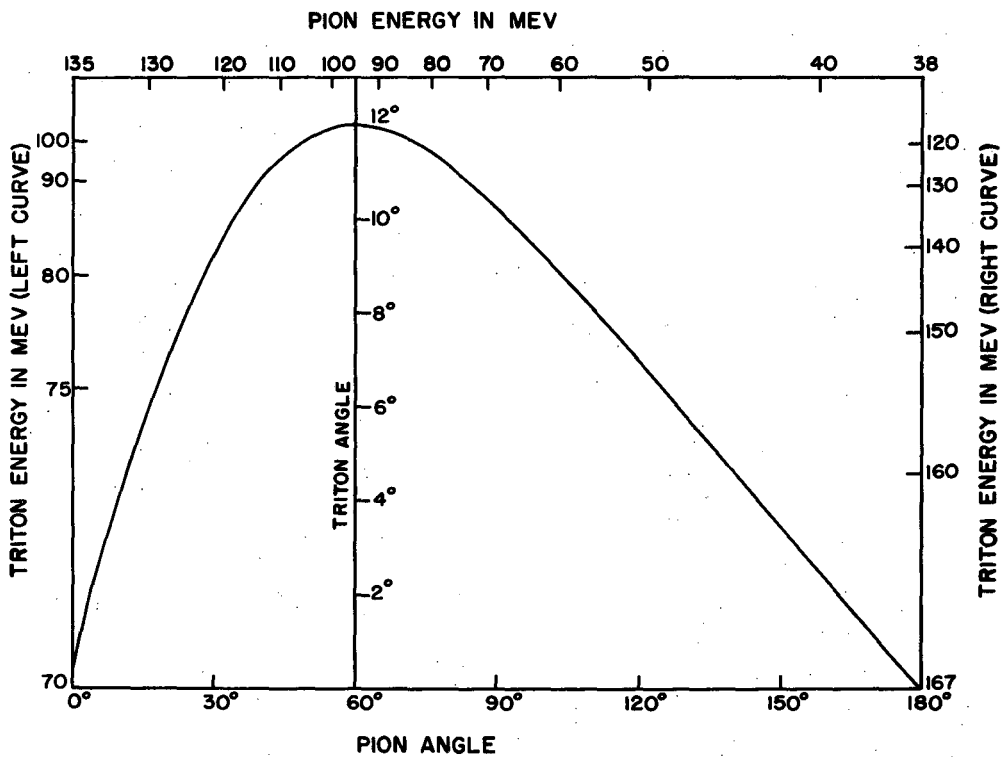
plotted giving the probability that a particle directed along θ before scattering will pass through the limits of the phosphor after scattering. Such functions can be calculated for both the pion and triton in both horizontal (or polar) and vertical (or azimuthal) directions. The horizontal plane is the plane containing the beam axis and the centers of all the counters. The net probability that both particles pass through their respective counters is then proportional to $h_{\pi}(\theta_{\pi}) \cdot v_{\pi}(\phi_{\pi}) \cdot h_t(\theta_t) \cdot v_t(\phi_t)$ where θ is the polar angle, ϕ is the azimuthal angle, h is the horizontal probability, and v is the vertical probability. Since θ_{π} , θ_t and ϕ_{π} , ϕ_t are correlated, the two h functions must be multiplied to give $H(\theta)$, and similarly the two v functions to give $V(\phi)$; the θ and ϕ refer to the angles of the particle counter that defines the solid angle. If the differential cross-section is assumed more or less constant over the counter, the total probability of intercepting both particles is given by the ratio of $\int H(\theta)V(\phi)\sin\theta d\theta d\phi$ integrated over all angles divided by $\int \sin\theta d\theta d\phi$ integrated over the counter. This numerical integration is simplified by using the fact that $\int H(\theta)V(\phi)\sin\theta d\theta d\phi$ is equal to $\int H(\theta)\sin\theta d\theta \cdot \int V(\phi)d\phi$, and that $\sin\theta$ can be assumed constant over the counter. The small angle scattering correction is the reciprocal of the interception probability.

VII. REFERENCES

1. M. Ruderman, Phys. Rev. 87, 383 (1952).
2. S. Bludman, to be published.
3. A. M. L. Messiah, Phys. Rev. 86, 430 (1952).
4. R. L. Garwin, Rev. Sci. Instr. 21, 569 (1950).
5. R. Madey, K. C. Bandtel, and W. J. Frank, unpublished measurements.
6. J. Carothers and C. G. Andre, Phys. Rev. 88, 1426 (1952).
7. W. Dudziak, Phys. Rev. 86, 602A (1952).
8. L. Neher, UCRL-2191.
9. F. Crawford, UCRL-2187 and M. L. Stevenson, UCRL-2188.
10. Durbin, Loar, and Steinberger, Phys. Rev. 84, 581 (1951).
11. R. Jastrow, Phys. Rev. 81, 165 (1951).
12. C. Weigand, Phys. Rev. 83, 1085 (1951).
13. D. Stork, private communication.
14. E. J. Williams, Proc. Roy. Soc. 169, 531 (1939).
15. Rossi and Greisen, Rev. Mod. Phys. 13, 240 (1941).
16. L. L. Eyges, Phys. Rev. 74, 1534 (1948).

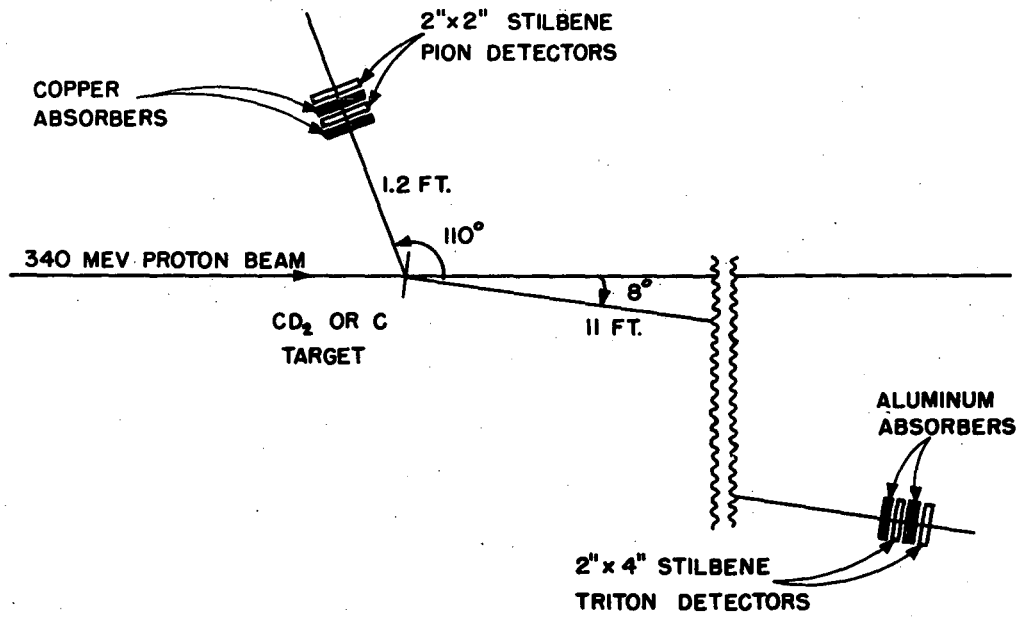
VIII. ILLUSTRATIONS

- Figure 1. Correlated angles and energies in the laboratory system for the process $p + d \rightarrow t + \pi^+$. The incident proton energy is 340 Mev.
- Figure 2. Experimental arrangement for observing the process $p + d \rightarrow t + \pi^+$.
- Figure 3. Circuit used to shape, limit, and add photomultiplier pulses.
- Figure 4. Germanium diode quadruple coincidence circuit.
- Figure 5. Time sequence of particles arriving at the counters. The time origin is taken as the arrival of a single radio-frequency proton pulse at the target.
- Figure 6. Angular correlation test for the process $p + d \rightarrow t + \pi^+$. The correlated angles are 8° for the triton and 110° for the pion.
- Figure 7. Time correlation test for the process $p + d \rightarrow t + \pi^+$. Zero time is based on pion and triton calculated times of flight.
- Figure 8. Range spectrum of particles arriving at the triton counters, and causing a coincidence.
- Figure 9. Experimental angular distribution for the process $p + d \rightarrow t + \pi^+$.
- Figure 10. Theoretical angular distributions for the process $p + d \rightarrow t + \pi^+$, compared with the experimental data.



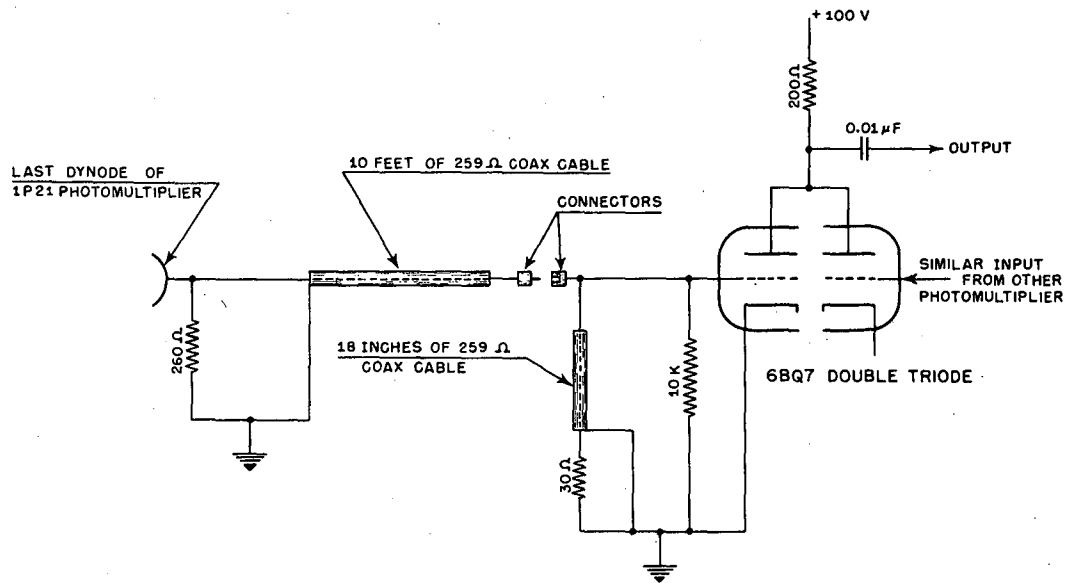
MU-4517

Fig. 1. Correlated angles and energies in the laboratory system for the process $p + d \rightarrow t + \pi^+$. The incident proton energy is 340 Mev.



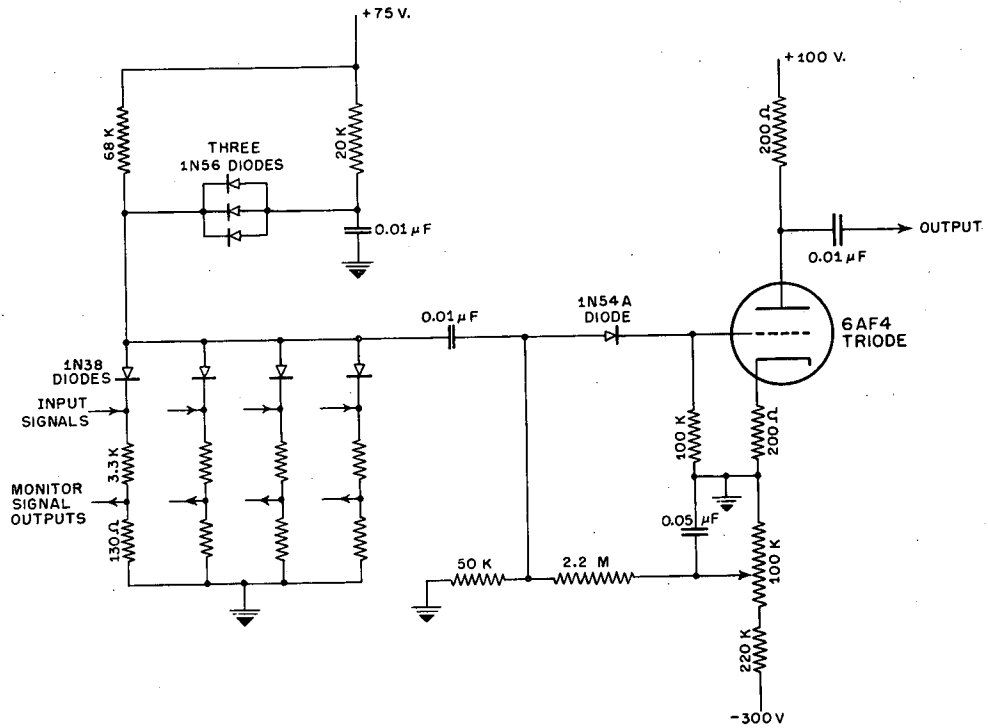
MU-4519

Fig. 2. Experimental arrangement for observing the process $p + d \rightarrow t + \pi^+$.



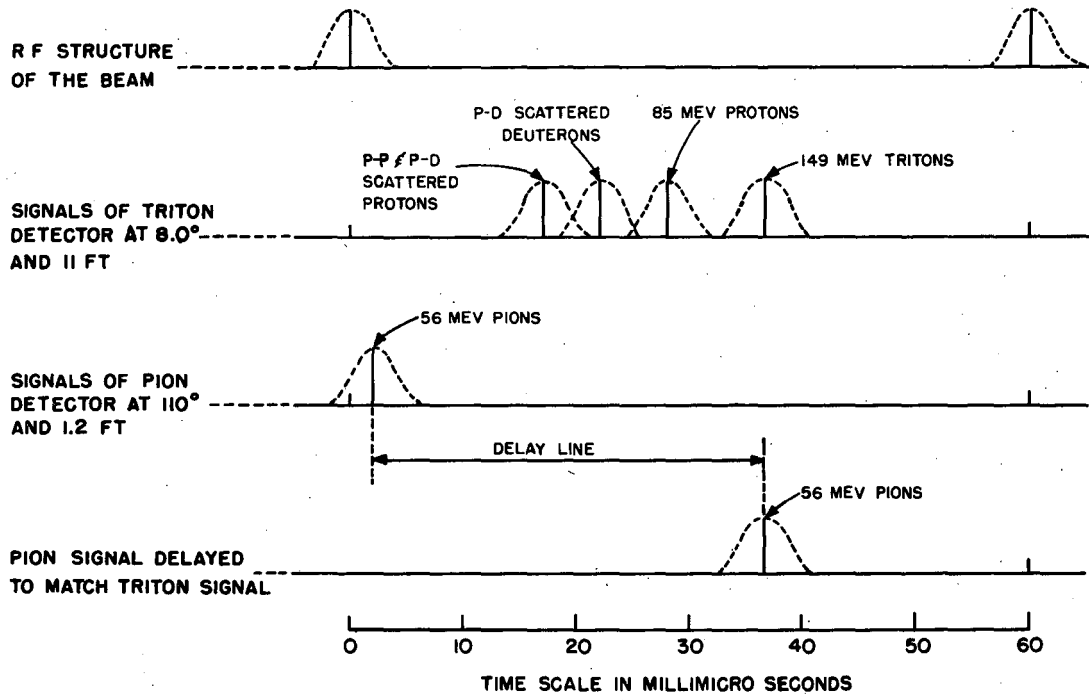
MU-5451

Fig. 3. Circuit used to shape, limit, and add photomultiplier pulses.



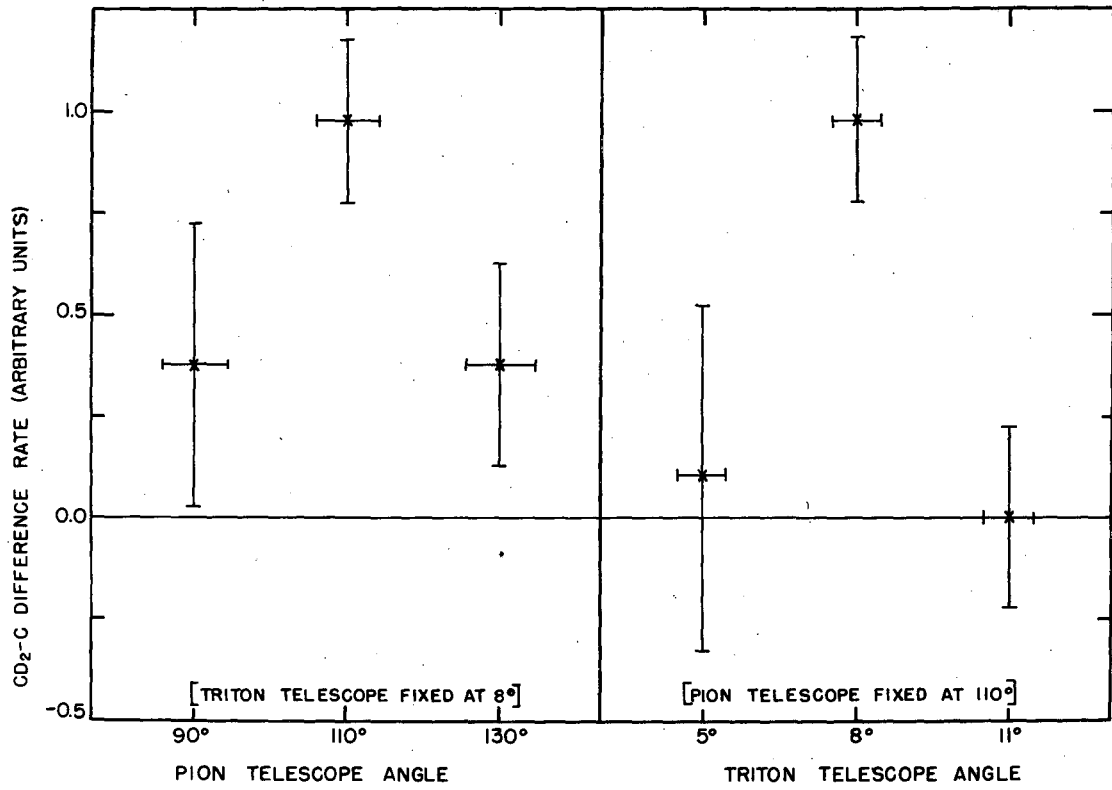
MU-5452

Fig. 4. Germanium diode quadruple coincidence circuit.



MU-4518

Fig. 5. Time sequence of particles arriving at the counters. The time origin is taken as the arrival of a single radio-frequency proton pulse at the target.



MU-3793

Fig. 6. Angular correlation test for the process $p + d \rightarrow t + \pi^+$. The correlated angles are 8° for the triton and 110° for the pion.

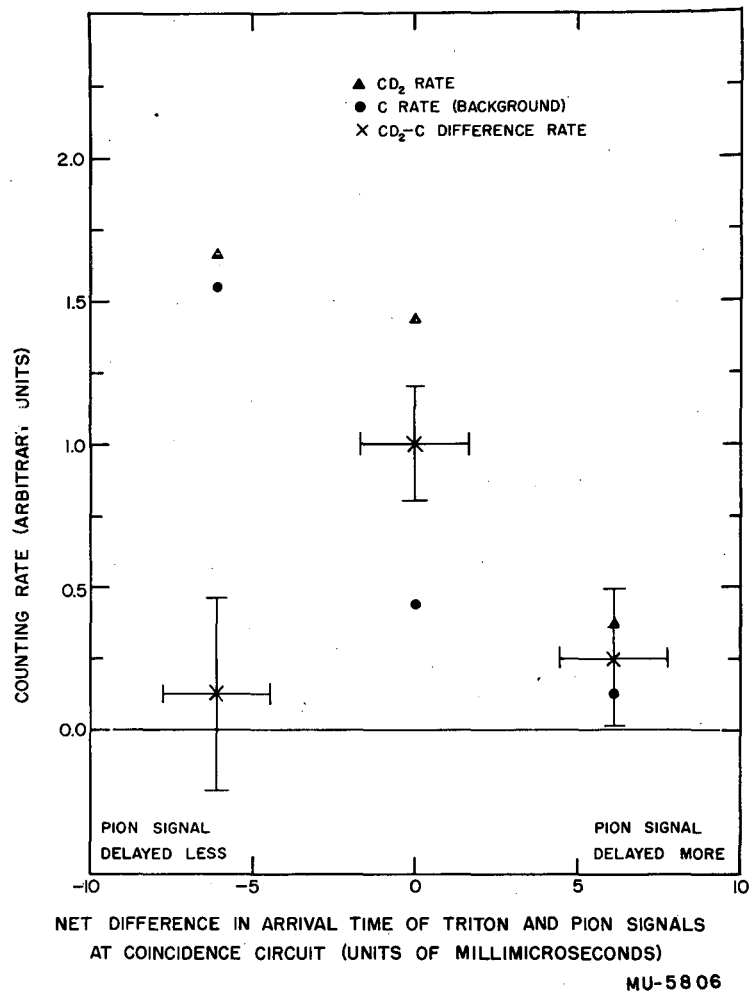
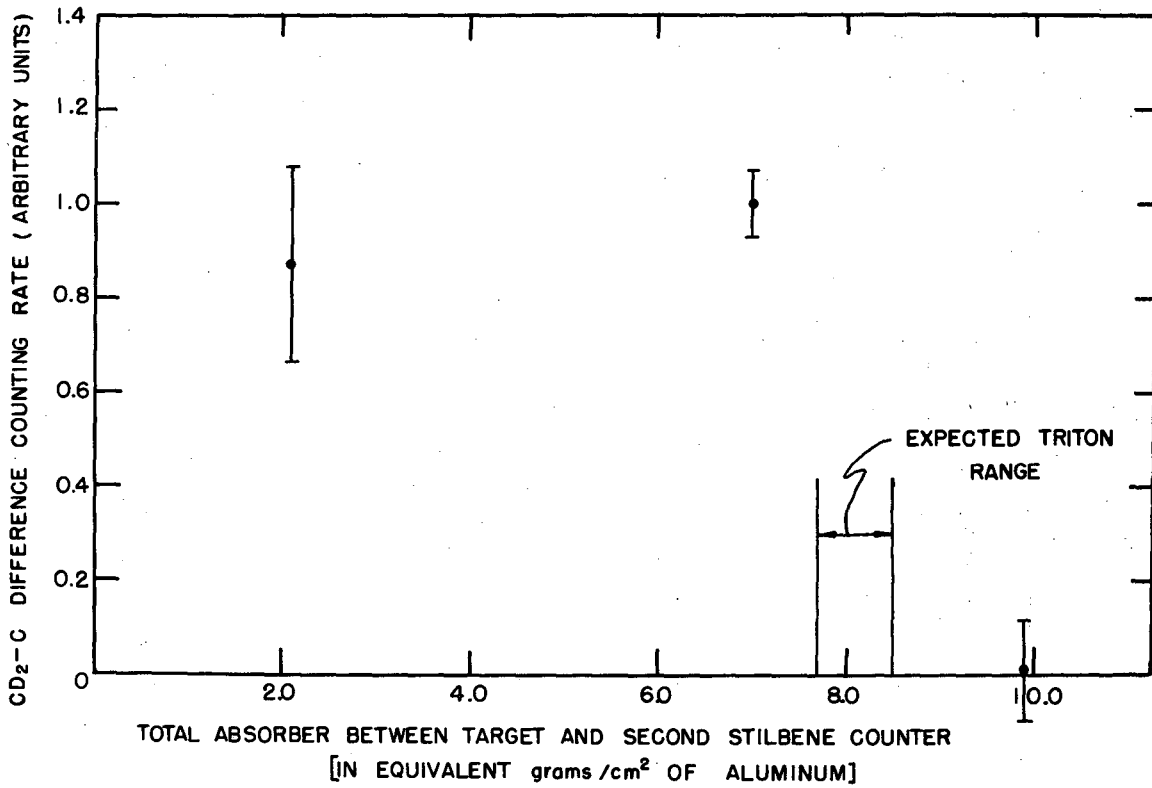


Fig. 7. Time correlation test for the process $p + d \rightarrow t + \pi^+$. Zero time is based on pion and triton calculated times of flight.



MU-4114 A

Fig. 8. Range spectrum of particles arriving at the triton counters, and causing a coincidence.

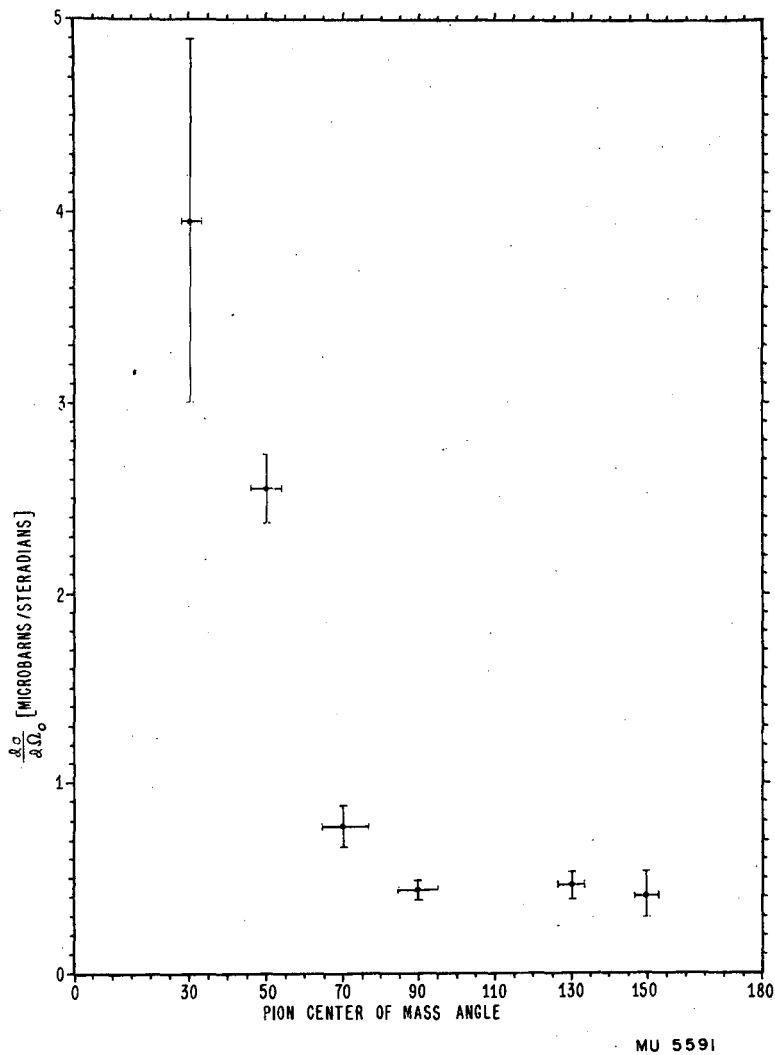


Fig. 9. Experimental angular distribution for the process $p + d \rightarrow t + \pi^+$.

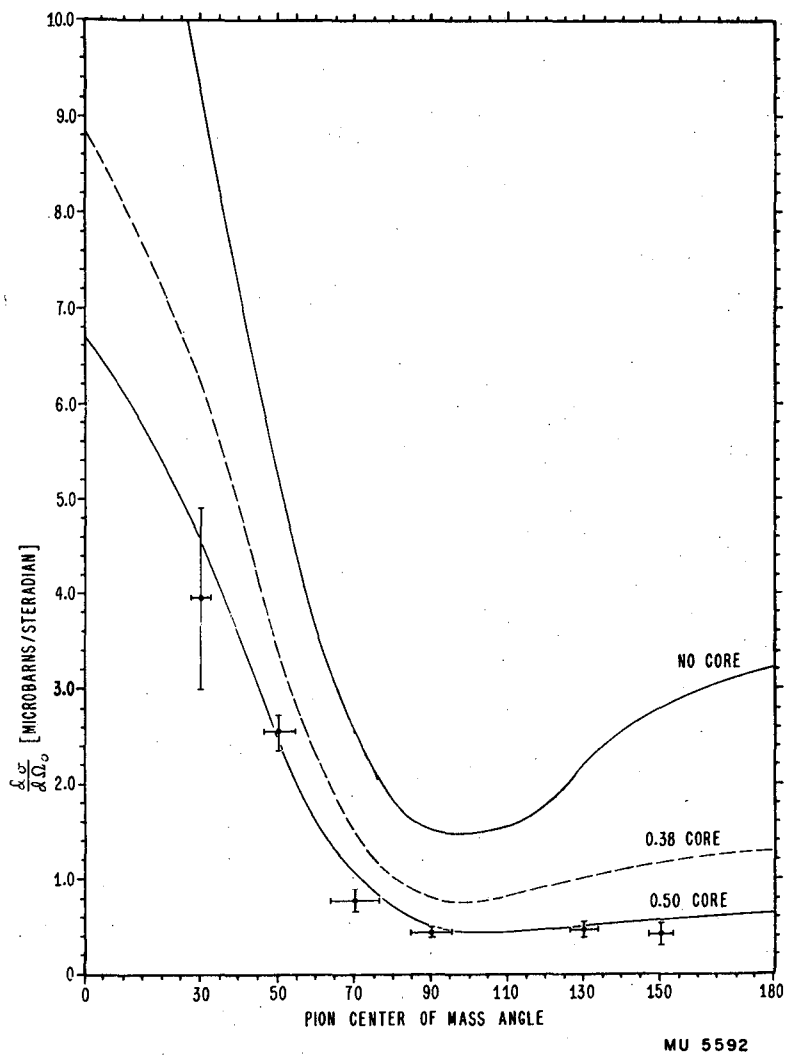


Fig. 10. Theoretical angular distributions for the process $p + d \rightarrow t + \pi^+$, compared with the experimental data.